

Research Paper

Design of Cellular Members under Axial-Shear-Flexure Interaction

Pattamad Panedpojaman¹, Worathep Sae-Long², Ruslan Yapa¹, Passagorn Chaiviriyawong¹

¹ Department of Civil and Environmental Engineering, Faculty of Engineering, Prince of Songkla University, Songkhla, 90112, Thailand, Email: ppattamad@eng.psu.ac.th (P.P.); 6510120037@email.psu.ac.th (R.Y.); cpassagorn@eng.psu.ac.th (P.C.)

² Civil Engineering Program, School of Engineering, University of Phayao, Phayao, 56000, Thailand, Email: worathep.sa@up.ac.th

Received November 10 2023; Revised February 22 2024; Accepted for publication April 18 2024.

Corresponding author: W. Sae-Long (worathep.sa@up.ac.th)

© 2024 Published by Shahid Chamran University of Ahvaz

Abstract. Due to lack of a design resistance for cellular beam-columns under the axial-shear-flexure interaction, the design interaction resistances were investigated through a validated finite element analysis. The beam-columns are simply supported and subjected to a mid-span point load and a compressive axial load, to provide the interaction. A modified interaction based on ANSI/AISC 360-16 and the shear design of SCI P355 were integrated to design the interaction resistance. In the parametric study of the interaction in various steel sections, the non-dimensional slenderness and opening parameters were examined. For beam-columns under high shear forces, Vierendeel mechanism and web-post buckling constitute the dominant failure modes depending on the opening parameters. Under high compression loads or flexural moment, flexural failure about the major axis is the dominant failure mode. However, the failure behaviors are generally combinations of the three modes. The design interactional resistance was examined in terms of failure shear forces computed from failure criteria of the three modes. Since design of the web-post buckling in SCI P355 does not consider effects of the interaction, their resistances are significantly higher than the FE results. The resistance is not governed by safety and requires modifications. On considering the co-existing actions in a quadratic interaction criterion, the proposed interaction resistance obviously complies with the FE results for cases of the web-post buckling failure, and agrees well with the FE results for cases of Vierendeel and flexural failure.

Keywords: Axial-shear-flexure interaction, Cellular beam-column, Interaction resistance, SCI P355, Web-post buckling.

1. Introduction

Cellular members, such as columns, beams, and frames, are intrinsic features in buildings. Extensive design guidelines and studies on elastic or inelastic stage are available to evaluate the load bearing capacity of cellular beams [1-5]. However, studies on load bearing capacity of cellular compressive members such as columns or beam-columns, with and without shear effects, are less accessible. Cellular columns under an axial-flexural load and without an external shear load have been studied with focus on their buckling resistance.

In elastic numerical studies of cellular or castellated columns, Sweedan et al. [6] and El-Sawy et al. [7] investigated the major-axis buckling load. Parametric studies were performed in their investigations by using finite element analysis. Failure assessment of the effects of web openings and column supports invited numerical solutions of the buckling loads. Analytical solutions on the elastic buckling of cellular columns about the major axis have been proposed [8-10]. The analytical buckling loads of pin-ended columns were validated with numerical analysis. Combined shear and flexural deformations around the opening were included in both the numerical and analytical solutions of the buckling load. Using nonlinear analysis, Sonck and Belis [11] investigated the buckling load of pin-ended cellular and castellated columns about the minor axis. Since cellular members are fabricated by cutting and re-welding steel sections, these processes cause imperfections and residual stresses in the cellular section. In addition to the flexural and shear deformations, the imperfections and residual stresses were included in the nonlinear finite element analysis to evaluate the buckling load. The results were compared with the EN 1993-1-1 resistance [12].

By suitable bracing in a plane frame design, buckling failure about the minor axis is prevented. Only the buckling load or the load-bearing capacity about the major axis is designed or considered. Under axial-flexure interaction, design interaction criteria of solid web steel sections such as ANSI/AISC 360-16 [13] and EN 1993-1-1 [12] have been normally applied to design the load bearing capacity, so-called interaction resistance, of cellular members about the major axis. The interaction resistance is computed by using critical sectional properties along the opening centerline. Under combined axial and flexural interaction, the efficiency of applying the AISC and EN methods to evaluate the interaction resistance of doubly symmetric cellular beam-columns with pin-pin support was examined in [14] by conducting a parametric set of finite element (FE) analyses. The design interaction resistance of cellular members was found to be unconservative or less conservative than that of regular members. Opening and web post geometries affect the conservatism level. When directly designing cellular members with the AISC and EN methods for them, some local behaviors around the opening are not considered. Therefore, the interaction resistance of the cellular members is overestimated.



Compared with the FE results at provided slenderness, the AISC deviation is less scattered than the EN deviation. Therefore, Panedpojaman et al. [14] proposed a modified (axial-flexure) interaction criterion based on the AISC method to reach more accurate interaction results.

Beam-column and frame members are generally subjected to combined axial, flexure and shear loads. Therefore, shear effects from an external shear load on the interaction resistance of members should be investigated. An analytical model for axial-shear-flexure interactions in steel members has been proposed in [15]. Under the shear-flexure interaction, the shear and flexural bending resistances of members tend to be degraded due to the co-existing actions. Design criteria for shear-flexure interaction are generally based on the interaction model of longitudinal unstiffened plate girders with slender webs, first proposed by Basler [16]. In the model, the shear resistance of the webs is affected by an applied flexural moment and must be reduced, once the applied moment is higher than the flange moment resistance.

In the current version of the design standards [12, 13], the resistance to axial-shear-flexure interaction has been considered, but with focus on cold-formed or hollow steel sections, not hot-rolled sections or cellular sections. There are no available studies concerning combined axial, shear and flexural loads of cellular members. For cellular members under high shear loads, web-post buckling as well as Vierendeel bending failure are considered the dominant failure modes. The web-post buckling tends to occur in cellular beams with narrow web posts. The Vierendeel bending failure is crucial in cellular beams with small Tee sections above and below the openings. Designs of web-post buckling and Vierendeel bending failure are guided by SCI P355 [3]. These behaviors may degrade the load bearing capacity of cellular beam-columns under the axial-shear-flexure interaction and should be investigated for safe designs.

Due to the limitations of design interaction resistance, this study aimed to investigate axial-shear-flexure interactions in cellular members. The investigation of interactions was conducted through FE analysis and validated against literature curated data for cellular specimens. The schematic configuration of the investigation is shown in Fig. 1. The interaction resistances about the major axis of a doubly symmetric cellular member with pin-pin support were scoped in this study. The members were applied subjected to a point load at the mid-span and a compressive axial load to provide the axial-shear-flexure interaction.

2. Design of Axial-Shear-Flexure Interaction

Nominal strength designs of ANSI/AISC 360-16 [13], and the shear design of SCI P355 [3] for cellular members were integrated to design the interaction resistance. Consider a member with an applied point load at the mid-span and a compressive axial load, P , and restrained to avoid buckling in the z direction as shown in Fig. 2. The member is subjected to combination of axial, shear and flexure loads. Flexural buckling can take place in the y direction. The deflection δ due to the primary moment, and a corresponding secondary moment $P\delta$ occur. For cellular members, the shear load, V , causes the key local responses, such as web-post buckling in the web post, or the Vierendeel mechanism in the tee sections above and below the opening.

2.1. Available Design for Regular Members

Based on the ANSI/AISC 360-16 methods [13], regular steel members subjected to an axial-flexure load should satisfy the criteria from Chapter *H* as given in Eq. (1). These are considered the flexural criteria. Doubly-symmetric members, not susceptible to torsion or distortional deformations are limited in the interaction criteria:

$$\frac{P}{P_n} + \frac{8}{9} \left(\frac{M'}{M_n} \right) \leq 1 \quad \text{for } P/P_n \geq 0.2$$

$$\frac{P}{2P_n} + \frac{M'}{M_n} \leq 1 \quad \text{for } P/P_n < 0.2$$
(1)

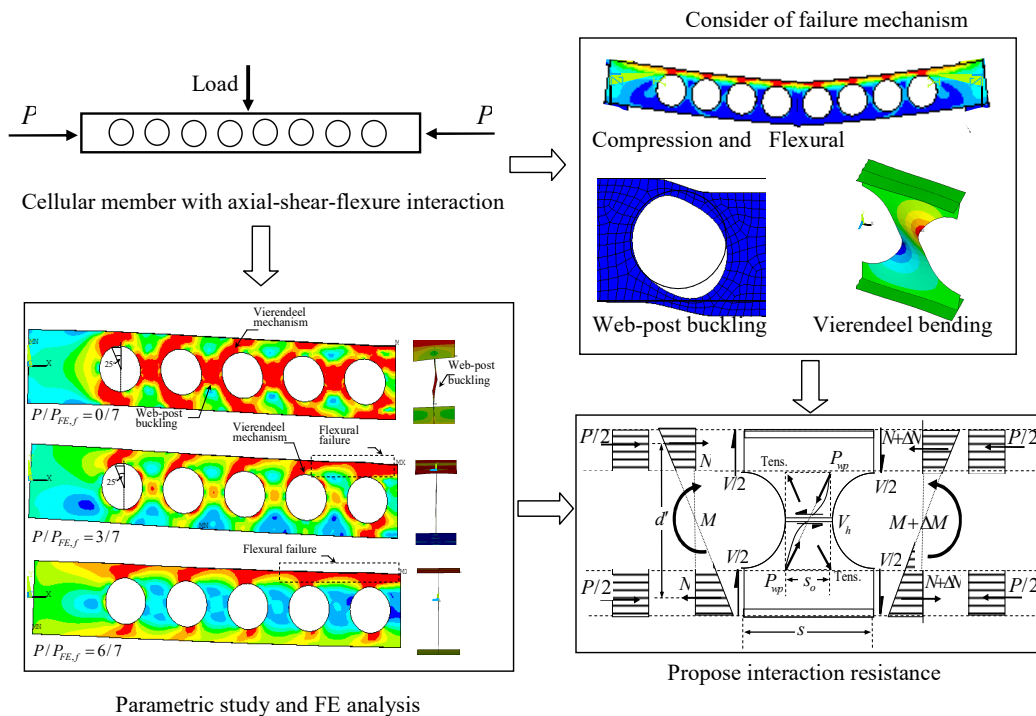


Fig. 1. The schematic configuration.



where P_n and M_n are the nominal axial and flexural strengths of the member, respectively, and M' is the flexural moment included as a secondary moment. Due to focusing on the ultimate load capacity, the safety factors for the nominal strength are not considered.

There are no specific criteria for members with combination of axial, shear and flexural loads for hot rolled or cellular steel. However, the ANSI/AISC 360-16 design code [13] provides the criteria for hollow steel members subject to combined forces in Eq. (2). Note that, for shear-flexural interaction responses of rectangular plates, a circular or rounded interaction equation has been proposed in prior studies [17, 18]:

$$\left(\frac{P}{P_n} + \frac{M'}{M_n}\right) + \left(\frac{V}{V_n}\right)^2 \leq 1 \quad (2)$$

$$V_n = 0.6f_y A_v C_v \quad (3)$$

where V_n is the nominal shear strength of the member in Eq. (3), f_y is the yield stress, A_v is the shear area of member sections and C_v is the shear coefficient of the web depending on its mechanical properties, shape, and shear buckling coefficient.

The flexural moment, M' , in Eqs. (1) and (2) is the sum of the primary moment from the load, M , and the secondary moment as given in Eq. (4). The term $C_m / (1 - P/P_e)$ is obtained from the second-order effect ($P - \delta$ effect):

$$M' = \frac{C_m}{(1 - P/P_e)} M \quad (4)$$

For the point load at the mid span, the theoretical value of C_m in Eq. (5) was used in the study. Note that, Appendix 8 of ANSI/AISC 360-16 [13] simplified C_m as $1 - 0.2P/P_e$:

$$C_m = 1 - 0.178P/P_e \quad (5)$$

where P_e is Euler's critical load for flexural buckling.

2.2. Available and Proposed Design for Cellular Members

Three failure behaviors namely flexural failure, web-post buckling, and Vierendeel bending failure, can occur in cellular members under axial-shear-flexure interaction. Once the shear effects are low or prevented, the flexural failure is dominant. Web-post buckling and Vierendeel bending failure are the critical failure behaviors of cellular members under high shear forces. Their proposed designs are described in this section. Due to focus on the ultimate load capacity, safety factors for the nominal strength are not considered.

2.2.1. Flexural failure (available design)

Without consideration of the shear effects, the flexural criteria in Eq. (1) were derived based on regular hot-rolled steel. However, it was found that the criteria tend to overestimate the load capacity for cellular columns, in [14], due to buckling around the opening. To achieve improved prediction accuracy, it was recommended that the AISC interaction criterion should be modified as given in Eq. (6) [14]. The modified interaction criterion was used in this study:

$$\frac{P}{P_{on}} + \frac{M'}{M_{on}} \leq 1 \quad (6)$$

where P_{on} and M_{on} are the nominal axial and flexural strengths of the cellular member, respectively, and M' is the flexural moment included as the secondary moment. For members with compact sections, M_{on} is the plastic moment capacity.

For cellular members, cross-sectional properties at the opening centerline (2T section method) were conservatively used for computing P_{on} and M_{on} , as shown in Fig. 3. The 2T section method generally provides a low value of the cross-section with openings. Therefore, the nominal axial and flexural strengths are conservative under the flexural behavior. The other methods such as Plain web section method, Surface weighting method, and Linear weighting method may be used to minimized the conservative results [5, 19].

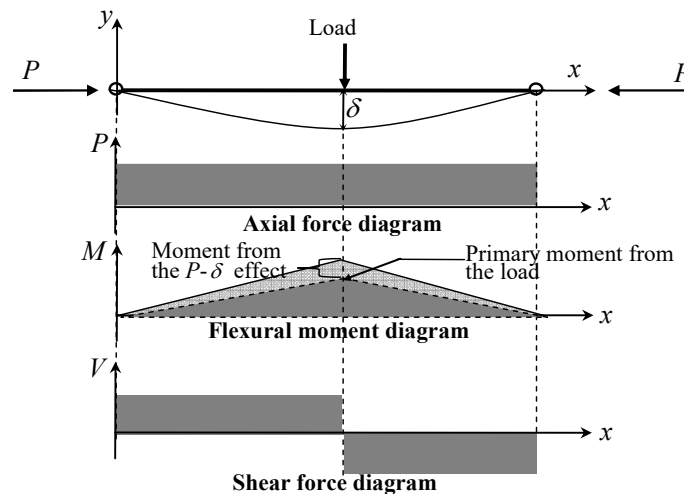


Fig. 2. Member with an applied point load at the mid-span and a compressive axial load.



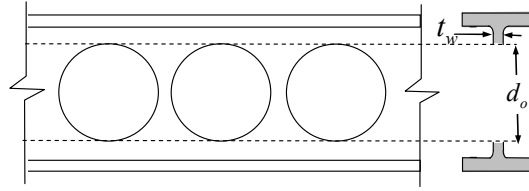


Fig. 3. Cross-section for computing the nominal strength.

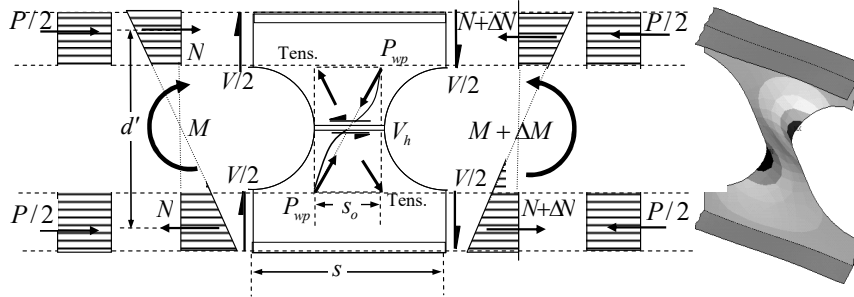


Fig. 4. Web-post buckling and co-existing actions.

Based on ANSI/AISC 360-16 [13], the nominal axial strength of cellular members is given in Eqs. (7) - (11):

$$P_{on} = (0.658^{\lambda^2} f_y) A_o \quad \text{for } \lambda^2 \leq 2.25 \tag{7}$$

$$\lambda = \sqrt{A_o f_y / P_e} \tag{8}$$

$$P_e = \frac{\pi^2 E I_o}{L_e^2} \tag{9}$$

$$A_o = A - t_w d_o \tag{10}$$

$$I_o = I - t_w d_o^3 / 12 \tag{11}$$

where λ is the non-dimensional slenderness in Eq. (8), A and A_o are the cross-sectional areas of non-perforated and perforated sections, respectively, E is the modulus of elasticity, I and I_o are the moments of inertia of non-perforated and perforated sections, respectively, L_e is the effective length for the buckling, d_o is the diameter of the opening, and t_w is the web thickness. For pin-pin supported members, L_e is the span length, L .

Once the point load w is applied at the mid-span, the primary shear force $V = w/2$ and the primary flexural moment $M = VL/2$ were used. The interaction criterion of the flexural failure including $P - \delta$ effect from Eq. (6) can be rewritten as:

$$\frac{P}{P_n} + \frac{C_m}{(1 - P/P_e)} \frac{(M \text{ or } VL/2)}{M_n} \leq 1 \tag{12}$$

2.2.2. Web-post buckling (proposed design)

Consider a web-post section subjected to axial, shear and flexural loads as shown in Fig. 4. Design of the web-post buckling based on SCI P355 [3] is explained first in this part. Note that SCI P355 [3] does not consider the compressive axial load. Both diagonal tensile and compressive forces act across the web-post. The diagonal forces constitute so-called strut action. The web-post is composed of a top and bottom part, as described in the figure. The compressive force on the strut, P_{wp} , is conservatively approximated by the horizontal shear force at the mid-height, V_h , ($P_{wp} = V_h$). For the web-post under a flexural moment, compression and tension forces occur in the top and bottom parts, respectively. The flexural force, N , is assumed to be located at the centroids of the critical Tees (at the opening centerline). V_h can be computed through the mechanical equilibrium in the top or bottom part as in Eq. (13):

$$V_h = \frac{Vs}{d'} \tag{13}$$

where d' is the distance between the centroids of the Tees at the opening centerline and s is the center-to-center spacing of adjacent openings.

To compute the buckling resistance of the web post, the buckling is assumed to occur over an effective length of the web, l_e , as given in Eq. (14). The area encountering to the compressive force is the critical web area of adjacent openings, A_{wp} , in Eq. (15). The moment of inertia of the web post, I_{wp} , is shown in Eq. (16):

$$l_e = 0.5\sqrt{s_o^2 + d_o^2} \tag{14}$$



$$A_{wp} = s_o t_w \quad (15)$$

$$I_{wp} = s_o t_w^3 / 12 \quad (16)$$

where s_o is the edge-to-edge spacing of adjacent openings. By substituting l_e , A_o and I_o with l_e , A_{wp} and I_{wp} , respectively, in Eqs. (7) to (9), the nominal buckling strength of the strut, P_{wpn} , can be derived. To prevent the web-post buckling, the nominal buckling strength of the web post, P_{wpn} , must exceed the compressive force on the strut, P_{wp} , ($P_{wp} < P_{wpn}$). In summary, the co-existing actions of the flexural moment and compressive axial load on the web-post buckling are not considered in the design method of SCI P355 [3].

Based on the parametric study in Section 4, without consideration of the co-existing actions, the design shear resistances for the web-post buckling are typically overestimated. This reflects the effects of the co-existing actions on web-post buckling. Furthermore, due to the interaction shown in Fig. 4, both flexural moments and axial forces cause an additional compressive force in the web post, especially in the top part. The additional compressive force may accelerate the buckling behavior. On the other hand, the web-post buckling also affects the flexural failure. The design resistance of SCI P355 [3] should be modified to incorporate the interaction effects.

The critical interaction occurs in the top part due to collaboration of the compressive force N and the compressive axial force P . In the current study, P was also assumed to be located at the centroids of the critical Tees. Therefore, the approximate compressive force on the strut, P_{wp} , and the nominal buckling strength of the strut, P_{wpn} , are the same. But the general moment-shear interaction in solid rectangular plates was applied. The interacting axial force N and P , and shear force V in the web post need to jointly satisfy this quadratic nonlinear criterion:

$$\left(\frac{V}{V_n}\right)^2 + \left(\frac{N}{N_{tn}} + \frac{P}{P_{on}}\right)^2 \leq 1 \quad (17)$$

where V_n is the nominal shear strength of the web post and N_{tn} is the nominal axial strength of the Tee section. Since the axial force N varies with the flexural moment, N/N_{tn} can be replaced with the moment ratio M'/M_{on} .

The equation is similar to the bending-shear interaction criterion for rectangular plates proposed in [17]. The shear failure of a web post is commonly by web-post buckling. Therefore, the nominal shear strength in Eq. (17) was considered the nominal shear strength for web-post buckling, $V_n = V_{wpn}$. Through the mechanical equilibrium in the top or the bottom part, the nominal shear strength for the web-post buckling V_{wpn} can be deduced from the nominal buckling strength of the web post P_{wpn} as shown in Eq. (18):

$$V_{wpn} = \frac{P_{wpn} d'}{s} \quad (18)$$

Based on the parametric study, for low shear forces ($V/V_{wpn} < 0.5$), the web-post buckling has a small contribution in the interaction. Instead, the mechanism of pure flexural behavior is critical. Therefore, the shear ratio is excluded from the interaction criterion for cases with low shear forces. Condition on low shear forces, affecting consideration of the shear effects, is also specified in the Vierendeel design of SCI P355 [3]. The criterion in Eq. (17) for the interaction in web-post buckling can be rewritten as in Eq. (19). By substituting M' from Eq. (4), the design shear resistance can be computed based on the criterion in Eq. (20):

$$\left(\frac{V}{V_{wpn}}\right)^2 + \left(\frac{M'}{M_{on}} + \frac{P}{P_n}\right)^2 \leq 1 \quad \text{for } \frac{V}{V_{wpn}} \geq 0.5 \quad (19)$$

$$\left(\frac{V}{V_{wpn}}\right)^2 + \left(\frac{C_m}{(1-P/P_e)} \frac{(VL/2)}{M_{on}} + \frac{P}{P_n}\right)^2 \leq 1 \quad \text{for } \frac{V}{V_{wpn}} \geq 0.5 \quad (20)$$

2.2.3. Vierendeel mechanism (proposed design)

A symmetric section with a circular opening at the mid-height is shown schematically in Fig. 5. The section is subjected to an axial force N , a compressive axial force P , and a shear force V . Transfer of the axial and shear forces across the opening causes the Vierendeel bending moment. Under a critical Vierendeel bending moment, yielding of the Tee sections above and below the opening promotes the formation of plastic hinges at the four corners. The moment and shear force in the section degrade the Vierendeel bending strength. To compute the net Vierendeel bending resistance of SCI P355 [3], the web thickness is subsequently reduced due to the shear force interaction and axial force interaction in a nonlinear manner. Many steps are required to design the net Vierendeel bending resistance. Furthermore, the interactions of the compressive axial load on the Vierendeel mechanism are not clearly considered in the design method of SCI P355 [3].

To simplify the computations, a linear or nonlinear interaction formula has been also applied instead the method of SCI P355 to account for the co-existing actions [20, 21]. Panedpojaman et al. [20] proposed a quadratic nonlinear criterion of the co-existing actions for evaluating their joint effects. Their Vierendeel bending resistance provides similar results obtained from SCI P355 [3]. However, the criterion is only based on the shear-flexure interaction, without considering the compressive axial load. The Vierendeel mechanism of [20] was modified to include effects of compressive axial load.

As the critical section for Vierendeel mechanism, the steel section above the opening is separated into two sides: the low and the high moment sides, as shown in Fig. 5. The sections from the opening centerline to the critical line were considered. Based on stress distributions in the sections under Vierendeel failure, the critical section varies and depends on the flexural moment and shear loads. The critical line at 25° from the opening centerline has been used [20-22]. For symmetric steel sections, the shear force V and the axial force N are equally resisted by the top and the bottom Tees. Due to the force transfer, locally three driving forces co-exist, namely shear force V_θ , axial force N_θ , and bending moment (the so-called Vierendeel bending moment) $M_{V,\theta}$ in the Tee section at the critical angle θ . The three driving forces were assumed to behave at the centroid of the Tee section as:



$$V_\theta = (V/2)\cos\theta \pm (N_{o^\circ})\sin\theta \tag{21}$$

$$N_\theta = (N_{o^\circ})\cos\theta \pm (V/2)\sin\theta \tag{22}$$

$$M_{V,\theta} = (V/2)((d_o + s_t)\tan\theta - \bar{y}_\theta \sin\theta) \pm (N_{o^\circ})(\bar{y}_\theta \cos\theta - \bar{y}_{o^\circ}) \tag{23}$$

where \bar{y}_θ is the distance from centroid to the top edge of the Tee section at the critical angle θ , and s_t is the depth of the Tee section at the opening centerline. The interacting shear force, axial force and Vierendeel bending moment in the critical Tee section are assumed to jointly satisfy this quadratic nonlinear criterion:

$$\left(\frac{V_\theta}{V_{tn,\theta}}\right)^2 + \left(\frac{N_\theta}{N_{tn,\theta}}\right)^2 + \left(\frac{M_{V,\theta}}{M_{tn,\theta}}\right)^2 \leq 1 \tag{24}$$

where $V_{tn,\theta}$, $N_{tn,\theta}$ and $M_{tn,\theta}$ are the nominal shear, axial, and moment strengths of the Tee section at the critical angle.

Since the Tee section area is critical at the opening centerline ($\theta = 0^\circ$), $V_\theta / V_{tn,\theta}$ and $N_\theta / N_{tn,\theta}$ were conservatively approximated by $(V/2) / V_{tn,0^\circ}$ and $N_{o^\circ} / N_{tn,0^\circ}$. $V_{tn,0^\circ}$ is half of the nominal shear strength of the perforated section at the opening centerline, V_{on} , ($V_{tn,0^\circ} = V_{on} / 2$). Furthermore, the axial force varies in line with the flexural moment M and the compressive axial load P . The N ratio at the opening centerline ($N_{o^\circ} / N_{tn,0^\circ}$) can be substituted with sum of the moment ratio M / M_{on} and the compressive P / P_{on} . Therefore, $V_\theta / V_{tn,\theta} \approx (V/2) / V_{tn,0^\circ} = V / V_{on}$ and $N_\theta / N_{tn,\theta} \approx M / M_{on} + P / P_{on}$.

The Vierendeel bending moment $M_{V,\theta}$ in Eq. (23) can be approximated by using a simplified moment arm and neglecting the axial force. The simplified moment arm was considered from location of the critical section. The simplified $M_{V,\theta}$ can be computed as $M_{V,\theta} = (V/2)(0.45d_o / 2)$ [23]. Sum of $M_{V,\theta}$ along the four critical sections is considered the Vierendeel bending moment of the opening, MV , as given in Eq. (25). Simplifications of MV are also adopted in SCI P355 [3]. The nominal moment strength of the critical Tee section $M_{tn,\theta}$ can be conservatively approximated by $1.17 M_{tn}$ [20]. M_{tn} is the nominal moment strength of the vertical Tee at the opening centerline. Sum of $M_{tn,\theta}$ along the four critical sections is also considered the nominal strength of Vierendeel bending moment, MV_n , as given in Eq. (26):

$$MV = 4M_{V,\theta} = V(0.45d_o) \tag{25}$$

$$MV_n = 4M_{tn,\theta} = 4(1.17M_{tn}) \tag{26}$$

Through the simplifications described above, the criterion of the interaction with Vierendeel mechanism in Eq. (24), including effects of the secondary moment, can be rewritten as:

$$\left(\frac{V}{V_{on}}\right)^2 + \left(\frac{M'}{M_{on}} + \frac{P}{P_n}\right)^2 + \left(\frac{MV}{MV_n}\right)^2 \leq 1 \tag{27}$$

By substituting M' from Eq. (4) and MV from Eq. (25), the design shear resistance can be computed based on the criterion in Eq. (28):

$$\left(\frac{V}{V_{on}}\right)^2 + \left(\frac{C_m}{(1 - P/P_e)} \frac{(VL/2)}{M_{on}} + \frac{P}{P_n}\right)^2 + \left(\frac{V(0.45d_o)}{MV_n}\right)^2 \leq 1 \tag{28}$$

In this study, the moment resistance of the Tee section and the perforated section were assumed to be at the plastic limit states. Because the co-existing actions are simultaneously considered in Eq. (27), there is no need to compute the individual reduction as specified in SCI P355 [3].

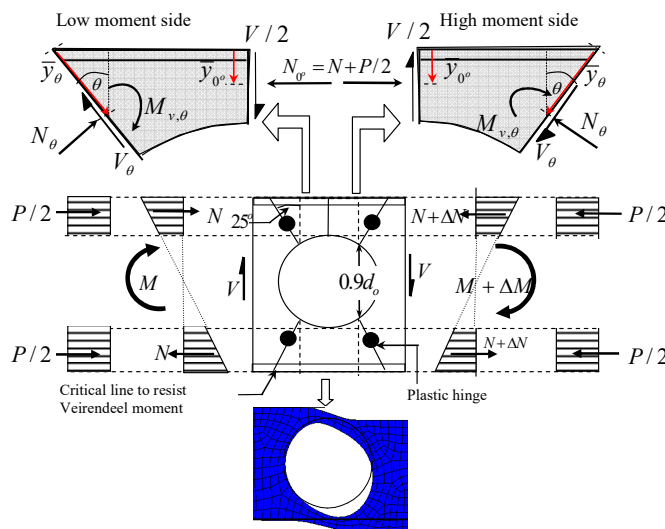


Fig. 5. Vierendeel mechanism and co-existing actions in steel section above the opening.



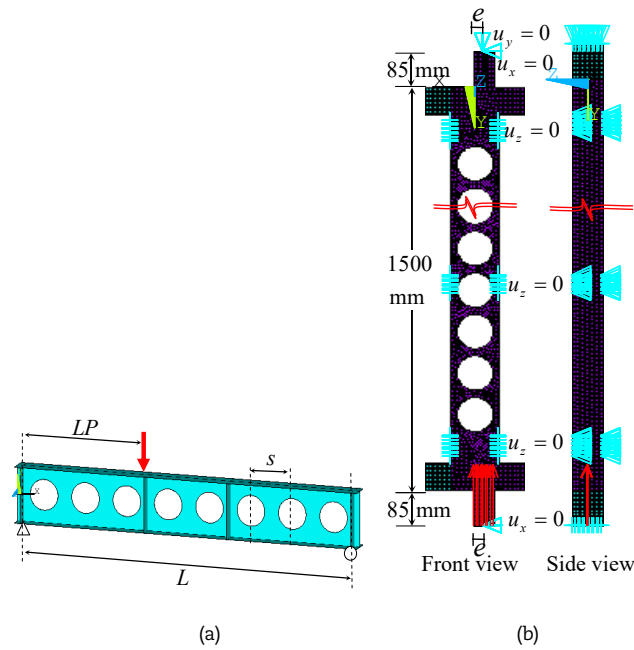


Fig. 6. Geometries of the specimens: (a) beams; and (b) columns.

3. Experimental Validation and Finite Element Simulation

To examine the combined flexure, shear and axial resistance of cellular members, finite element analysis was used in the parametric study. The finite element simulations were validated against literature curated data of cellular beams and columns. The beam specimens are under combined flexure and shear loads, whereas the column specimens are under combined flexure and axial loads. To the authors' knowledge, there are no available experiments concerning the combined axial, shear and flexure loads of cellular members.

3.1. Experimental Validation

The finite element simulations were validated against literature curated data for 12 cellular beams [24-27] and 6 cellular columns [14]. The cellular beam specimens are simply-supported beams subjected to point loads. The Vierendeel failure or the web-post buckling occurs in the opening nearest to the point load, since the moment and shear in the opening are more critical than around the far side openings. The specimen geometries are described in Fig. 6(a), and documented in Table 1. For all specimens, some lateral supports were set to prevent the lateral torsional buckling. Details of the lateral supports are reported in the literature. The case labels NB and CB refer to perforated and cellular beams, respectively. The specimen parameters are as follows: H is the section depth; t_f and b_f are the flange thickness and width; t_w is the web thickness; s is the opening spacing; L is the span length of the beam or column; LP is the distance from the left support to the point load; and f_y are the yield stresses. Note that f_y is an average of the yield stresses of web and flange. To prevent a concentrated stress, web stiffeners were set at the locations of the point load and the supports for most specimens.

The column specimens are doubly symmetric cellular columns with pin-pin support and a 1,500-mm length, as illustrated in Fig. 6(b). Buckling loads of the specimens about the major axis were investigated. To provide co-existing actions of flexural moment and compression load, an eccentric compression loading was applied. Stiffeners at the specimen ends were welded to transfer the load to the columns. The total length of the tested column is 1,670 mm including the 85-mm height of the ball support at both ends. The lateral supports about the minor axis were set to prevent lateral deflection. Therefore, all column specimens failed by flexural buckling about their major axis. The specimen geometries are documented in Table 2. The case label CC refers to cellular column and e is the eccentric distance.

Table 1. Details of the literature curated experimental cellular beams.

Specimen	H (mm)	b_f (mm)	t_f (mm)	t_w (mm)	s (mm)	d_o (mm)	L (m)	LP (m)	f_y (MPa)	Ref. Tested by
NB1	449.8	152.4	10.9	7.6	410	315	1.70	$L/2$	367.5	[24]
NB2	449.8	152.4	10.9	7.6	378	315	1.70	$L/2$	367.5	[24]
NB3	558	180	13.5	8.6	480	358	1.90	$L/2$	300*	[25]
NB4	599	300	24.0	13.5	485	422	1.94	$L/2$	300*	[25]
NB5	600	180	13.5	8.6	485	430	1.94	$L/2$	300*	[25]
CB1	289.8	133.2	7.8	5.7	300	200	3.10	$L/2$	319	[26]
CB2	289.8	133.2	7.8	5.7	300	200	5.50	$L/3, 2L/3$	338.5	[26]
CB3	309.3	133.2	7.8	5.7	300	225	3.80	$L/2$	333.5	[26]
CB4	309.3	133.2	7.8	5.7	300	225	5.60	$L/3, 2L/3$	368.5	[26]
CB5	435	101.6	7.0	5.8	450	300	3.80	$L/2$	360	[26]
CB6	435	101.6	7.0	5.8	450	300	4.20	$L/3, 2L/3$	340	[26]
CB7	394.5	113	14.1	9.4	389	286	2.83	$L/2$	285	[27]

Note: * Assumed yield strength for steel grade S235 = 300 MPa [28].



Table 2. Details of the literature curated experimental cellular columns.

Specimen	H (mm)	b_r (mm)	t_r (mm)	t_w (mm)	s (mm)	d_o (mm)	L (m)	LP (m)	f_y (MPa)	Ref. Tested by
CC1	88	51	4.8	3.2	76	64	1.67	20	314	[14]
CC2	88	51	4.8	3.2	76	64	1.67	40	314	[14]
CC3	88	51	4.8	3.2	76	64	1.67	60	314	[14]
CC4	108	63	4.8	3.2	96	80	1.67	20	314	[14]
CC5	108	63	4.8	3.2	96	80	1.67	40	314	[14]
CC6	108	63	4.8	3.2	96	80	1.67	60	314	[14]

3.2. Finite Element Simulation

By using the ANSYS software, nonlinear three-dimensional finite element (FE) simulations were run in the parametric study. As described in Section 3.1, the simulation was validated against the experimental results. The 4-node shell element, SHELL181, was used to simulate steel sections. The element is suitable for a thin steel plate. Based on a sensitivity study of the load–deflection curve, the element size of about $H/20$ was meshed in the FE simulation. The boundary conditions and the geometry of the specimens were simulated based on the experimental details. The investigated FE simulation is a simply-supported beam and a pin-ended column. For the column models, parts of the ball support with 85-mm height were simulated as a rigid plate and linked to the column ends. To prevent minor axis displacements (lateral displacements), the columns were restrained as reported in the literature.

Due to effects of residual stresses from fabrication of cellular members, the undeformed members were perturbed by an initial imperfection [29, 30]. The imperfection is generally based on the first mode of elastic eigenvalue analysis. Therefore, an eigenvalue analysis was required to set the imperfection of the members before analyzing inelastic behavior. In the eigenvalue analysis, small point loads were applied to the mid-span in the beam cases, whereas small equal but opposite end compression forces were applied to the column ends in the column cases. In this study, the buckling mode corresponds to web buckling for the beams (the specimens with shear loads) whereas the buckling mode corresponds to flexural buckling for the columns (the specimens with compression loads). After the eigenvalue analysis, an inelastic analysis was conducted. The imperfection amplitude $H/500$ [31] and $L/500$ [14] were applied to undeformed geometry for the beams and the columns, respectively, as shown in Figs. 7(a) and 7(b). Note that the imperfection size can cover the effects of residual stresses [29, 30].

The yield stress was obtained from coupon testing, giving elastic modulus of 200 GPa, inelastic modulus of 2 GPa ($0.01E_s$) after yielding, and Poisson's ratio of 0.3, which were set in the FE analysis. To determine the yield point, the Von Mises yield criteria were used. The Newton-Raphson iterative method and time step analysis were used to control the analysis. In order to achieve convergence, size increment of the applied load was automatically reduced. The minimum load increment of associated with the minimum time step size. The minimum load increment near the failure is about 0.1 kN and the normal time step size is 200.

3.3. Validation

Similar to the experimental results, the failures in FE beam simulations were by web post buckling for specimens NB1-5, and by Vierendeel mechanism for specimens CB1-7. Examples of the main failure modes are illustrated in Figs. 8(a) and 8(b). For the web-post buckling, the buckling S shape and the concentrated stress in the web post can be observed in Fig. 8(a). For the Vierendeel mechanism, the concentrated stresses in the four corners of the openings occur, extending to the top and bottom flanges as shown in Fig. 8(b). The main failure mode of the column specimens CC1-6 was overall buckling about the major axis, as shown in Fig. 8(c). Under compression load, yielding of the columns occurs only in the compression flange. Lateral torsional buckling could not be found in the FE behavior, due to the minor-axis movement being prevented.

The experimental and FE load–deflection curves are compared in Fig. 9. The experimental load–deflection curves are generally in line with the FE curves. The failure point loads for the beam specimens and the failure compression loads for the column specimens are summarized in Table 3. For both the beam and column specimens, the FE failure loads agree well with the experimental data. However, the FE failure load is slightly higher than the experiment, by about 2% on an average. The deviation of the FE curves from the experimental curves may be because of limitations in simulating actual test data, such as inaccuracy of the material stress-strain curve, imperfections, boundary conditions, residual stresses, etc. Note that the failure modes are mainly determined by the load conditions and the experimental geometries, not the initial imperfections.

It can be observed that geometric configuration of the cellular section affects the interaction resistance of cellular members. The specimens are limited to select axial forces, shear forces or flexural moment. Effects of the geometric configurations and the co-existing actions should be further investigated to propose a suitable design under axial-shear-flexure interaction. Due to limitation of data available to investigate suitable designs, a FE parametric study was performed.

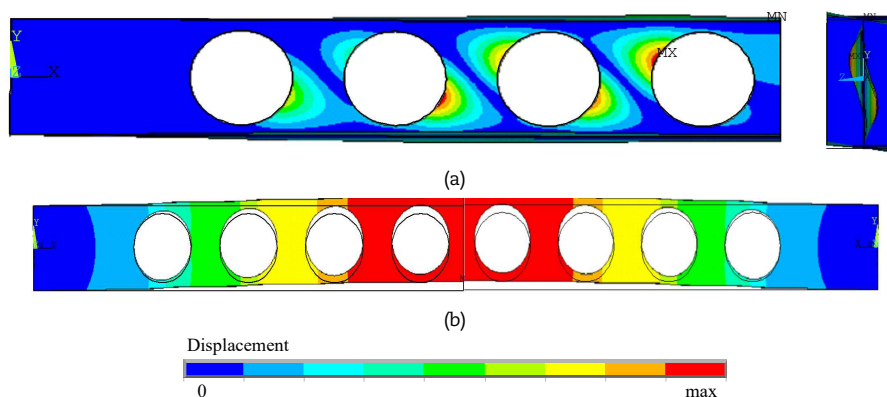


Fig. 7. Elastic buckling mode for the imperfection: (a) web buckling for specimen with shear loads; and (b) global buckling for specimen with compression loads.



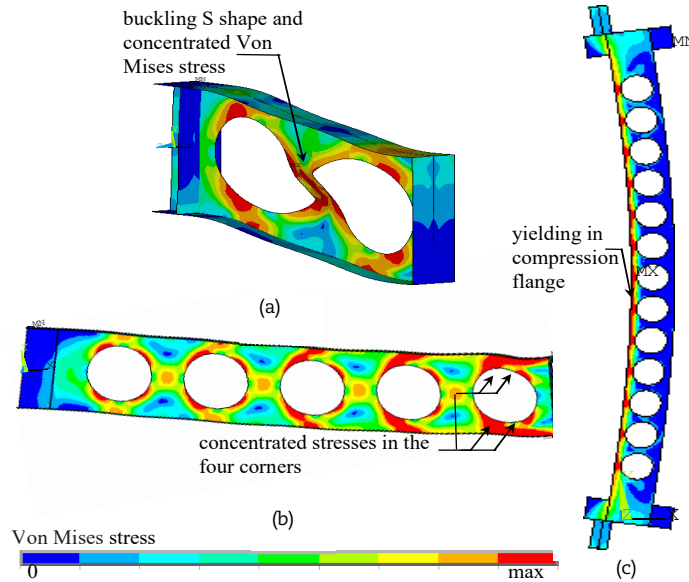


Fig. 8. Failure modes of the FE models: (a) web-post buckling in NB1; (b) Vierendeel mechanism in CB1; and (c) overall buckling in CC1.

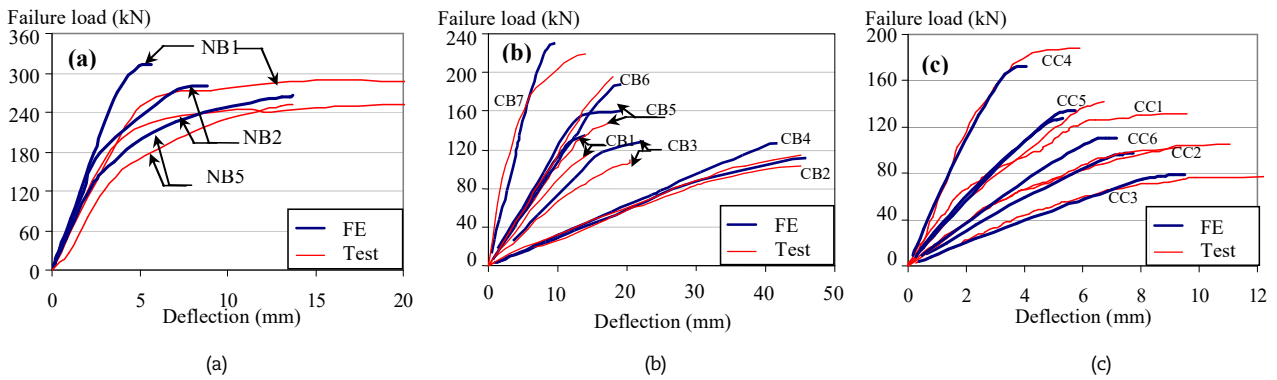


Fig. 9. Comparison of the load- (lateral) deflection curves: (a) Specimens NB1-5; (b) Specimens CB1-7; and (c) Specimens CC1-6.

Table 3. Failure loads of the specimens experimentally and from the FE simulations.

Specimen identifier	Failure load (kN)		FE load / Test load
	Test	FE	
NB1	288	314	1.09
NB2	256	276	1.08
NB3	536	464	0.87
NB4	626	680	1.09
NB5	264	266	1.01
CB1	120	130	1.08
CB2	108	112	1.04
CB3	112	122	1.09
CB4	118	124	1.05
CB5	152	160	1.05
CB6	194	190	0.98
CB7	218	224	1.03
CC1	129	126	0.97
CC2	103	96	0.93
CC3	77	77	1.01
CC4	184	171	0.93
CC5	137	133	0.97
CC6	100	109	1.09
	Average		1.02

Note: Failure loads are shear loads for the beams and compression loads for the columns.



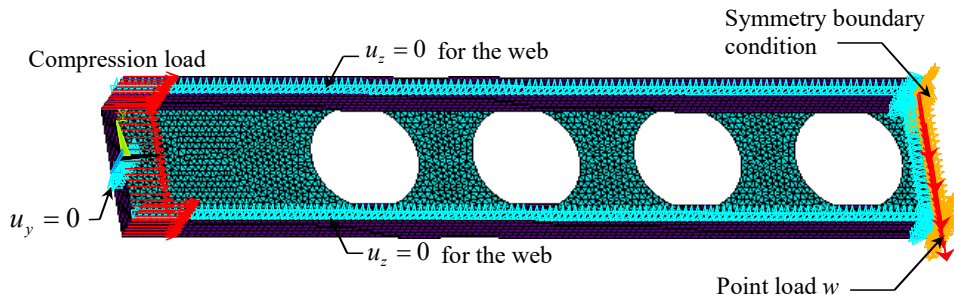


Fig. 10. FE model for investigating the axial-shear-flexure interactions.

4. Parametric Study of Axial-Shear-Flexure Interaction

The axial-shear-flexure interactions of members are examined in this section. Simply supported members with various section geometries were simulated for the assessment. Both regular (no opening) and cellular beam-columns were included in this study. Accuracy of the proposed design method was evaluated for the load capacity under the axial-shear-flexure interactions by comparing with numerical FE simulation results.

4.1. Investigated Cases and Simulations

FE simulations for investigating the axial-shear-flexure interactions are shown in Fig. 10. For the loading, a range of axial compression loads at the supported end was applied to the beam-columns. The moment and shear loadings were applied via a point load at the mid-span. Owing to the symmetry of the beam-columns, only half of their length was simulated to reduce the computational cost. Therefore, the supported end was set as a pin-ended support ($u_y = 0$) whereas the other side was assumed mirror symmetric. To avoid minor-axis (lateral) displacements, the web was restrained ($u_z = 0$). For simulations of cellular beam-columns, distances from the support ends to the nearest openings edges were specified to be $1.5d_0$ to prevent local failure around the nearest openings. Stress transfer from the end solid section to the opening section may cause a local failure [14].

The element type, imperfections and analysis of the FE simulations have been described in the previous section. The steel yield stress, f_y , of 355 MPa (steel grade S355) and the elastic modulus of 200 GPa were employed for all simulations. To conservatively investigate the failure load, the perfectly plastic stage was specified after yield.

In the parametric study, various steel sections with and without web openings, the non-dimensional slenderness, and opening parameters such as spacing and opening ratios, were examined as follows:

- Steel sections: IPE400, HEA400, HEB400, IPE600, HEA600, and HEB600. The selected sections are compact sections. The section ratios, A_f / A_w , are 1.52, 2.94, 3.03, 1.24, 2.14, and 2.15, respectively. The web slenderness ratios, d / t_w , are 46.5, 35.5, 29.6, 50.0, 45.4 and 38.7, respectively. A_f and A_w are the total flange and web area of the sections, respectively. d is the section depth before fabricating to cellular beam-columns.
- Spacing ratio s / d_0 : no opening, 1.2 and 1.5.
- Opening ratio d_0 / d : no opening, 0.8, 1.0 and 1.2.
- Non-dimensional slenderness λ : about 0.3 and 0.7 representing the short and long members, respectively.

Effects of the section ratio and the web slenderness ratios on failure behavior of cellular beams have been found in [20, 30, 31]. Values of these ratios represent normal cases of hot-rolled steel sections. Note that section depth of the cellular members, H , was simulated corresponding to the fabricating process. The web slenderness ratios of the cellular members, H / t_w , are shown in Table 4.

The FE buckling load of the member subjected to a pure compressive axial load, $P_{FE,f}$, was examined first. Eight compression loads, P , for the $P / P_{FE,f}$ ratios 0, 1/7, 2/7, 3/7, 4/7, 5/7, 6/7, and 1, were simulated to plot curves of the axial-shear-flexure interactions. A total of 96 solid web beam-columns and 576 cellular beam-columns were simulated.

Accuracy of the AISC method in estimating the nominal strength of regular and cellular columns has been investigated in [14]. Comparing with the FE buckling load, the design P_n is generally conservative with the maximum conservatism level of 21.9%. The slenderness ratio and the section ratio affect the conservatism level of the design P_n . Therefore, accuracy of the design P_n was not further investigated in this study and only effects of the axial load on the design shear and flexural moment resistances were focused on. The maximum V and M , which satisfy the criteria in Section 2, are considered as the interaction shear and flexural moment resistance, V_{ds} and M_{ds} , respectively.

Table 4. Web slenderness ratios of the cellular members.

Section	d / t_w	H / t_w					
		$s / d_0 = 1.2$			$s / d_0 = 1.5$		
		d_0 / d			d_0 / d		
		0.8	1.0	1.2	0.8	1.0	1.2
IPE400	46.5	64.7	69.3	73.8	62.6	66.6	70.7
HEA400	35.5	49.4	52.9	56.4	47.8	50.9	53.9
HEB400	29.6	41.2	44.1	47.0	39.9	42.4	45.0
IPE600	50.0	69.6	74.5	79.4	67.3	71.7	76.0
HEA600	45.4	63.2	67.6	72.1	61.1	65.1	69.0
HEB600	38.7	53.9	57.7	61.5	52.1	55.5	58.8



4.2. Regular Beam-Column

The failure in simulation under the interaction load was generally in the flexural failure mode about the major-axis, with an example shown in Fig. 11. The local buckling around the web is secondary behavior, especially for short members with high shear loads. The design shear and flexural moment resistances (V_{ds} and M_{ds}) satisfied the flexural criterion in Eq. (12) and were compared with the FE failure shear or moment load (V_{FE} or M_{FE}). To investigate effects of the interaction, the design resistances and the FE failure load were normalized with their design nominal strengths (V_n or M_n). Variations of the normalized shear (V_{FE}/V_n and V_{ds}/V_n) and moment (M_{FE}/M_n and M_{ds}/M_n) resistance with the compression ratios ($P/P_{FE,f}$ or P/P_n) are plotted in Figs. 12(a) and 12(b) for λ of 0.3 and 0.7, respectively.

As seen in Figs. 12(a) and 12(b), the design shear resistance is conservative compared with the FE shear resistance for both small and large λ . The section ratio, A_f/A_w , affects the conservatism level. As observed in Fig. 12, the HEB400 beam-columns ($A_f/A_w = 3.03$) provide the highest conservatism level whereas the IPE600 beam-columns ($A_f/A_w = 1.24$) provide the lowest conservatism level. For HEB400 beam-columns, the maximum differences of the normalized design and FE shear resistance ($(V_{ds} - V_{FE})/V_n$) are 10.9% and 4.8% for λ of 0.3 and 0.7, respectively. Effects of the section ratio on the conservatism level may be due to inaccuracy in predicting the nominal shear strength for the flange part. The AISC method does not consider the shear strength of the flange part. The flange area is relatively large, for sections with a large section ratio, affecting the shear strength. Therefore, a more conservative shear strength is provided in such cases.

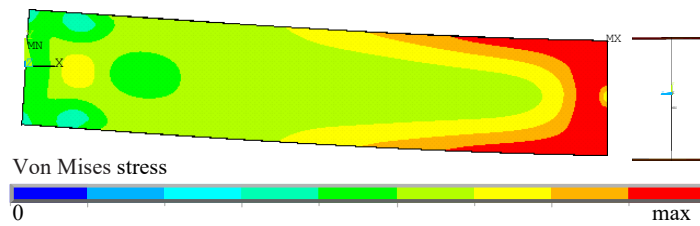


Fig. 11. Failure behavior of HEB400 with λ about 0.3 and $P/P_{FE,f} = 0$.

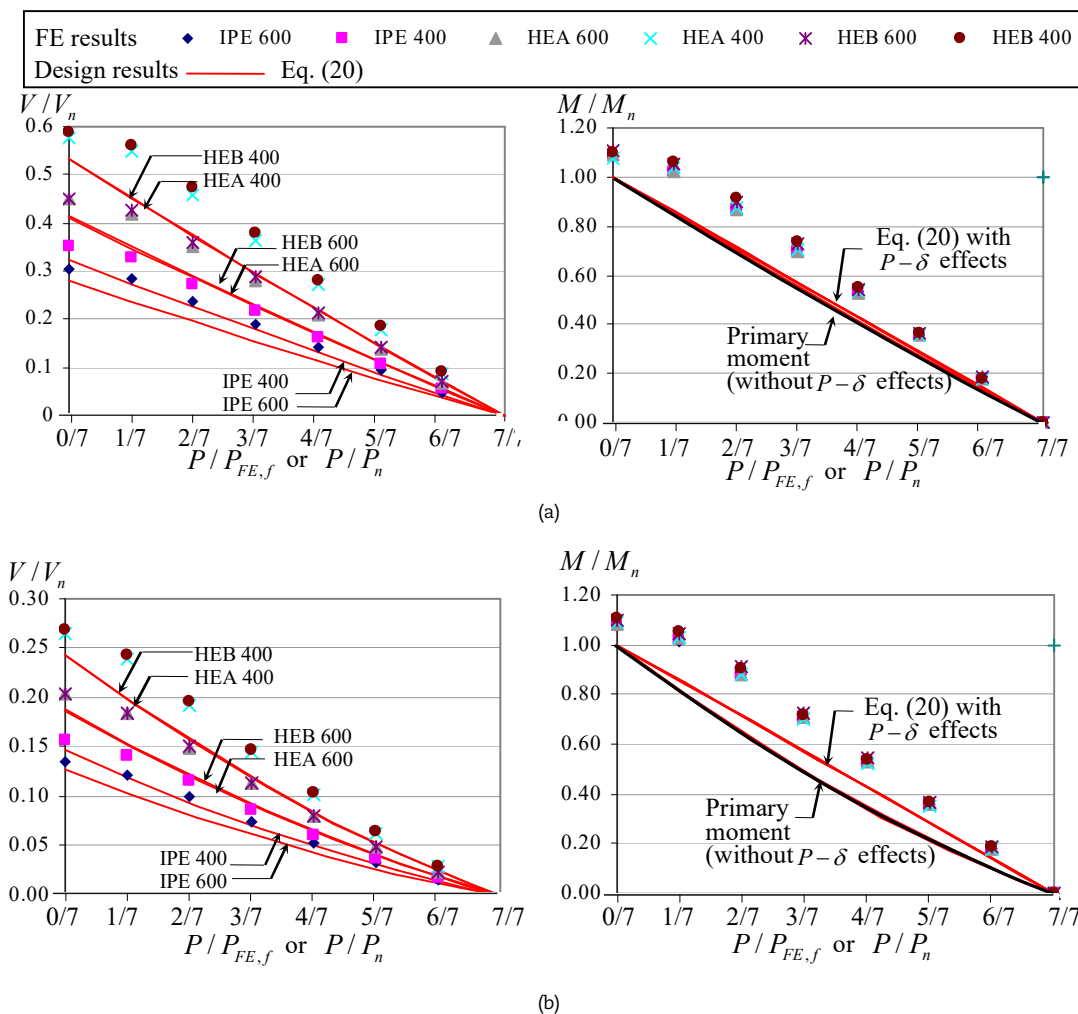


Fig. 12. Variations of the normalized (FE and design) shear and moment resistances with the compression ratios: (a) λ of 0.3; and (b) λ of 0.7.



The normalized moment resistance in Fig. 12 again shows that the design interaction moment resistances are overall conservative compared with the FE shear resistances for both small and large λ . The steel section affects the moment resistance relatively less. The maximum differences of the normalized design and FE moment resistances $((M_{ds} - M_{FE}) / M_n)$ for the beam-columns under low compression loads ($P / P_n \approx 0.1-0.4$) are 20.7% and 22.0% for λ of 0.3 and 0.7, respectively. The buckling behavior and the $P - \delta$ effect degrade the conservatism level at high compression loads ($P / P_n > 0.4$). Therefore, the design resistances are conservatively close to the FE resistances at such high compression loads. The conservatism level also reflects the conservative prediction of the nominal shear and flexural strengths. It is noted that without shear effects the FE moment strength is also generally higher than M_n , as reported in [14, 20].

In summary, for the investigated regular beam-columns, the flexural criterion without consideration of the shear interaction as given in Eq. (12) generally provides conservative resistances under axial-shear-flexure interactions.

4.3. Cellular Beam-Column

For short beam-columns (λ of 0.3), failure shear forces are higher compared with the long cases. Since effects of the opening parameters on failure behaviors of cellular beam-columns are similar, analytical results of some representative cases are shown. On varying $P / P_{FE,f}$, the shape deformation and Von Mises stress distributions of short HEB400 cellular beam-columns (λ of 0.3) with the largest opening portion ($s / d_o = 1.1$ and $d_o / d = 1.2$) and the smallest opening portion ($s / d_o = 1.5$ and $d_o / d = 0.8$) are shown in Figs. 13(a) and 13(b), respectively. Behaviors of the web-post buckling, Vierendeel mechanism, flexural failure, and their combinations, can be observed in Fig. 13. Shear behaviors, such as web-post buckling and Vierendeel failure, are dominant. The web-post buckling obviously occurred for beam-columns with narrow web-post ($s / d_o = 1.2$). Vierendeel bending failure is clearly critical for beam-columns with small Tee section above or below the openings ($d_o / d = 1.0$ and 1.2). Under high compression loads or flexural moments, the major-axis flexural failure is still the dominant failure. However, the failure generally combined all three behaviors. Note that, when Vierendeel failure occurs, the critical line at 25° of Vierendeel mechanism can be approximated for the interaction with and without the axial load as shown in Fig. 13. Therefore, the critical sections can be used to consider both Vierendeel bending moment and resistance.

The long beam-columns (λ of 0.7) are commonly under high flexural moment. Therefore, flexural failure about the major axis is the generally dominant failure, especially at a high compression load, $P / P_{FE,f} > 0.4$. Pure flexural failure is tensile yielding at the bottom flange and compression yielding or buckling at the top flange. Under axial compression loads, compressive stress reduces tensile stress in the bottom flange. Therefore, the tensile stress does not reach yielding. The opening parameters such as s / d_o and d_o / d affect the failure behavior less. However, at a low compression load the shear force affects the failure more. Therefore, the web-post buckling, Vierendeel mechanism, or their combination, occurs as shown in the examples of Figs. 14(a) and 14(b), respectively.

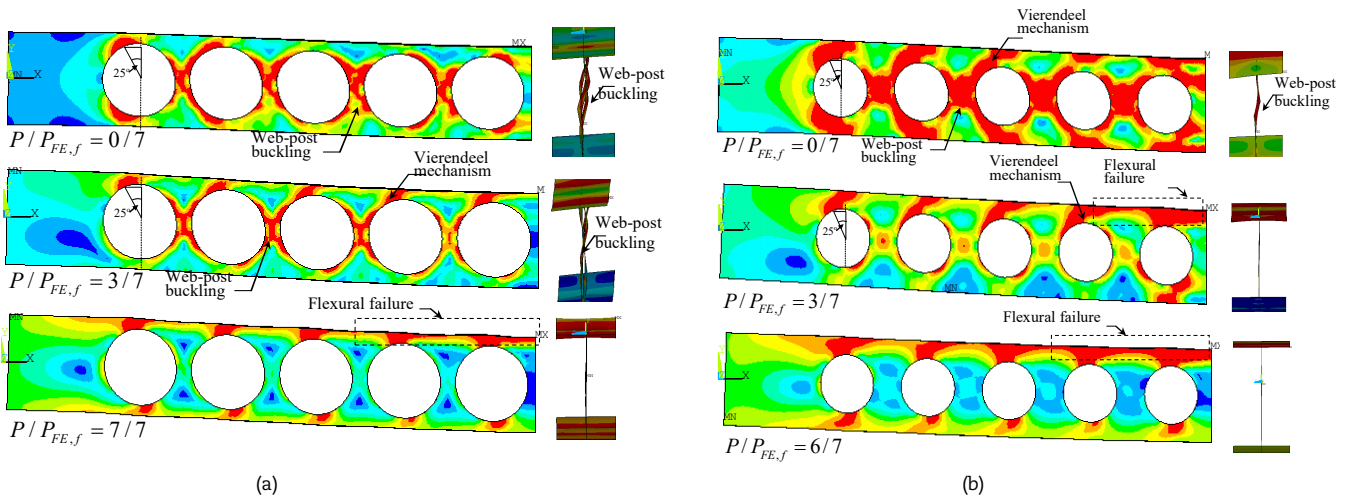


Fig. 13. Shape deformation and Von Mises stress distributions of short HEB400 cellular beam-columns with various $P / P_{FE,f}$: (a) with $s / d_o = 1.2$ and $d_o / d = 1.2$; and (b) with $s / d_o = 1.5$ and $d_o / d = 0.8$.

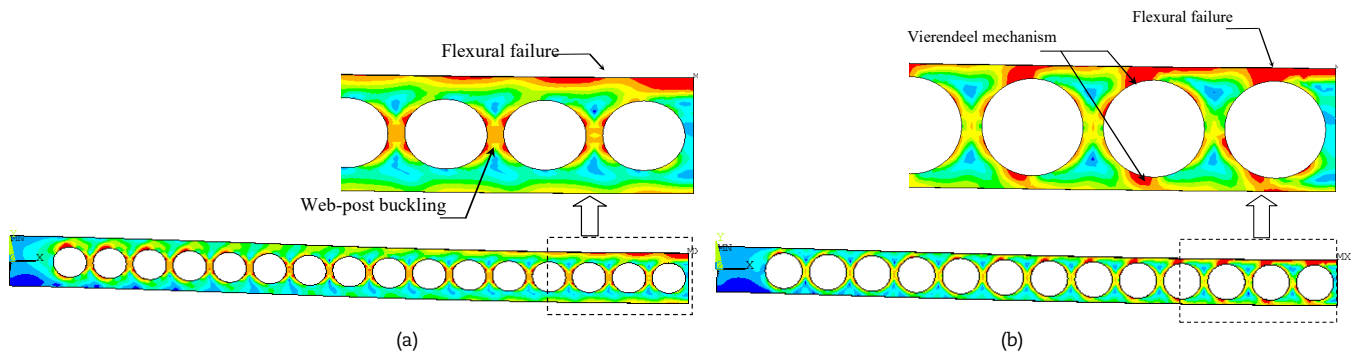


Fig. 14. Shape deformation and Von Mises stress distributions of long cellular beam-columns HEB400 with $P / P_{FE,f} = 0$: (a) with $s / d_o = 1.2$ and $d_o / d = 0.8$; and (b) with $s / d_o = 1.2$ and $d_o / d = 1.2$.



To investigate the design resistances of cellular beam-columns under the interaction load, the three failure behaviors were considered. Since shear forces are constant along the simulated beam-columns (see Fig. 2), all the web-posts have the same critical level, except the web-post at the mid-span which has a stiffener to distribute the concentrated load and the shear load. On the other hand, the flexural behavior and Vierendeel mechanism are critical at the mid-span and the opening nearest to the mid span, respectively, due to the relatively high flexural moments there.

To evaluate the efficiency of the design criteria, the shear force satisfying the criteria, so-called interaction shear resistance, was assessed. The FE failure shear load (V_{FE}) and the design shear resistance (V_{ds}) of HEB400 and IPE600 with varying opening portion (s/d_o and d_o/d) and λ of 0.3 and 0.7 are plotted with the compression ratios ($P/P_{FE,f}$ or P/P_{on}) in Figs. 15(a) and 15(b). The design shear resistances were computed from the three failure criteria for flexural failure, web-post buckling, and Vierendeel mechanism. For design purposes, the critical shear resistance of the three behaviors was further used to check against the applied shear load.

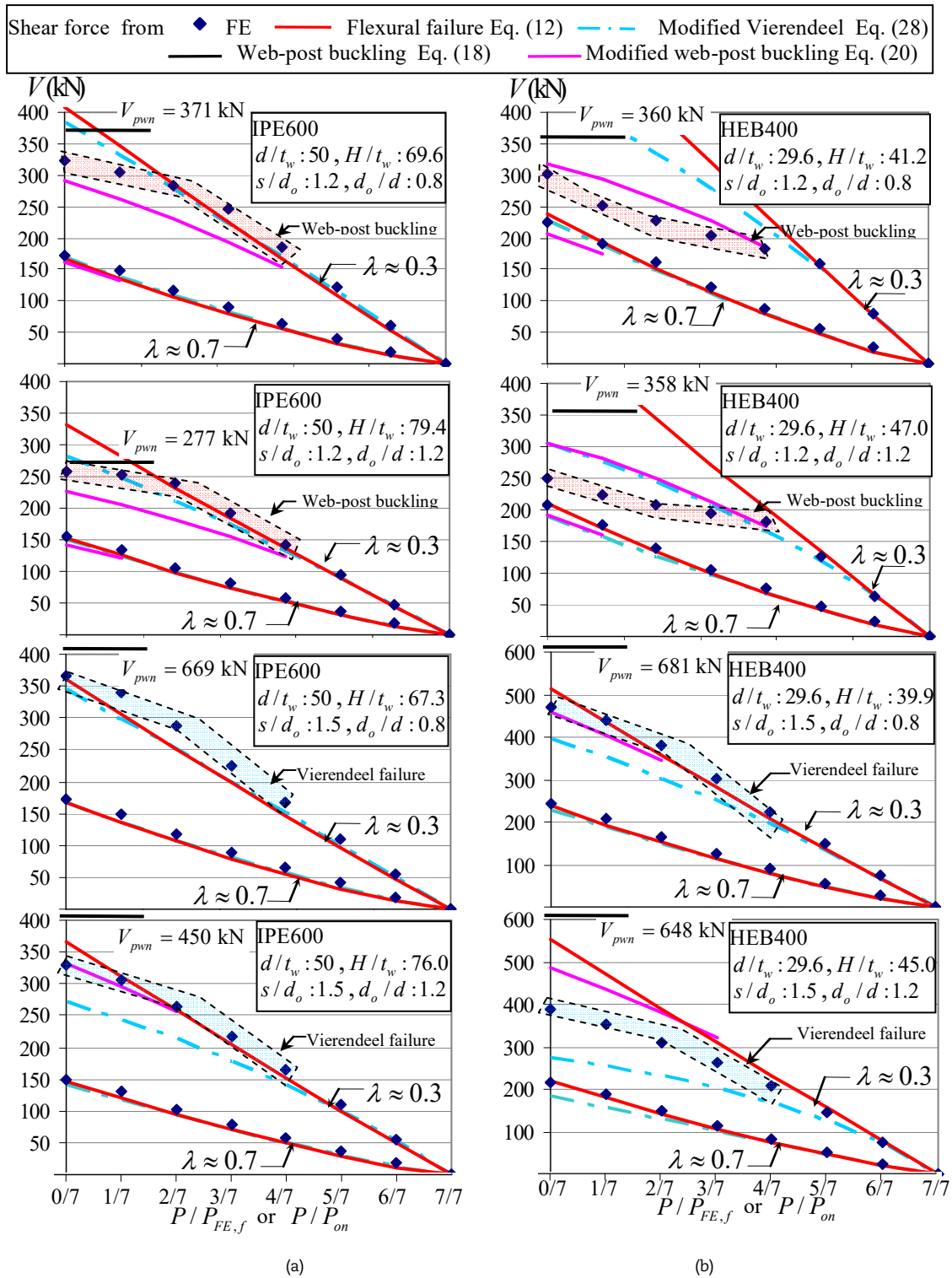


Fig. 15. Shear resistances of IPE600 and HEB400 obtained from alternative methods.



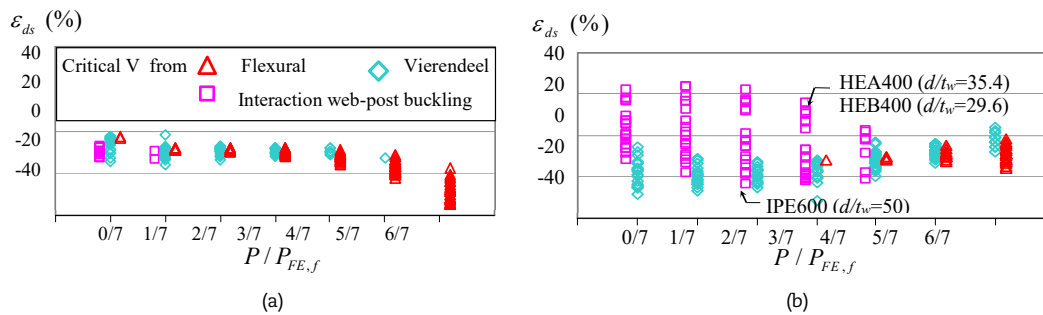


Fig. 16. Differences of the design shear resistances from the FE failure shear load: (a) long cellular beam-columns; and (b) short cellular beam-columns.

For the long beam-columns, the design shear resistances based on the flexural criterion in Eq. (12) or Vierendeel mechanism criterion in Eq. (28) conservatively agree well with the FE results. For the short beam-columns under high compression loads ($P/P_{FE,f} > 0.4$), the design shear resistance based on the flexural behavior or the Vierendeel mechanism conservatively agrees well with the FE results. Since the failure shear loads are high for the short beam-columns under low compression loads, web-post buckling or Vierendeel mechanism dominate their failure, as shown in Fig. 15. For Vierendeel mechanism failure, the design shear resistance tends to be overly conservative for cases with high section ratios, such as the HEB400 beam-columns. This is possibly due to poor accuracy of the nominal shear strength prediction. The web-post buckling and Vierendeel mechanism failure mainly depend on level of the compression load and the opening parameters (s/d_o and d_o/d), but not the web slenderness ratios d/t_w or H/t_w . It can be observed in Fig. 15 that the failure modes are still different for the sections having similar values of H/t_w .

In cases of the web-post buckling failure ($s/d_o = 1.2$), the design shear resistance of SCI P355 [3], without consideration of the co-existing actions given in Eq. (18), is significantly greater than the FE results. Overestimates by more than 50% can be clearly observed from the curves of HEB400 beam-columns with $s/d_o = 1.2$ in Fig. 15(b). This reflects the effects of the co-existing actions in web-post buckling criterion. The design shear resistance for the web-post buckling of SCI P355 [3] may not be safe and should be modified. The proposed design resistance with consideration of the co-existing actions given in Eq. (20) provides better results more in line with the FE results, for cases with web-post buckling failure.

For all cellular beam-columns, differences ε_{ds} of the critical design resistances from the FE resistances at a given compression load ($\varepsilon_{ds} = (V_{ds} - V_{FE})/V_{FE}$) are plotted with $P/P_{FE,f}$ in Fig. 16. The critical design resistances in the figure are the minimum shear resistances of the three failure behaviors. As shown in Fig. 16(a), for the long beam-columns, Vierendeel mechanism and flexural failure behavior are more critical than web-post buckling. It can be observed that web-post buckling and Vierendeel mechanism are commonly critical for short beam-columns in Fig. 16(b). The flexural behavior is typically critical for high compression loads.

The differences are in the range from -2.1% (conservative) to -36.0% for the flexural behavior, from -23.8% to +23.7% (overestimated) for the interaction criterion of web-post buckling, and from -32.0% to +3.6% for Vierendeel mechanism. Generally, the design resistances are in line with the FE results. For the flexural behavior, the resistances are significantly conservative for long beam-columns under very high compression loads ($P/P_{FE,f} > 0.7$). The reason may be a force cancellation between the direct compression load and the tensile forces from the flexural moment. The resistances to Vierendeel mechanism are normally conservative. The conservatism level agrees well with the investigation of cellular beam-columns without compression load, in [20]. For the web-post buckling, the conservatism level depends on the web slenderness ratio of d/t_w , not H/t_w . The resistances tend to be overestimated for sections with low web slenderness ratio (such as HEB400 having $d/t_w = 29.6$) and conservative for sections with high web slenderness ratio (such as IPE600 having $d/t_w = 50$). This may indicate that SCI P355 [3] tends to overestimate the shear strength of web-post buckling for low web slenderness ratios.

5. Conclusion

To investigate the flexure-shear-axial behavior and resistance of cellular members, a validated finite element (FE) analysis was used in a parametric study. Simply supported members with various steel sections, the non-dimensional slenderness ($\lambda = 0.3$ and 0.7), and opening parameters such as spacing and opening ratios were varied in the simulations. For the loading, a range of axial compression loads at the supported end was applied. The moment and shear loading were applied by a point load at the mid-span. Both regular (no opening) and cellular beam-columns were included in this study. A total of 96 solid web beam-columns and 576 cellular beam-columns were simulated. The design interaction resistance based on failure criteria of SCI P355 and ANSI/AISC 360-16 was modified to consider co-existing actions. The proposed formulae for resistance estimation were compared with the FE failure loads. Conclusions are as follows:

- For regular beam-column, the simulations generally gave flexural failure modes about the major-axis. The flexural failure criterion without consideration of the shear interaction typically provides conservative moment and shear resistances compared with the FE failure loads. The conservatism level reflects the conservative prediction of nominal shear and flexural strengths.
- For short cellular beam-columns ($\lambda = 0.3$), shear behaviors, such as Vierendeel failure and web-post buckling are dominant. The web-post buckling mainly occurred for beam-columns with narrow web-posts. Vierendeel bending failure is definitely crucial for beam-columns with small Tee section above or below the openings (i.e., with large openings). Under high compression loads or flexural moments, flexural failure is still the dominant failure. However, the failures are generally combinations of the three behaviors. In case of long cellular beam-columns ($\lambda = 0.7$), the beam-columns are typically under high flexural moment. Therefore, flexural failure is the dominant failure, especially at high compression loads. The opening parameters affect the failure behaviors less. The web-post buckling, Vierendeel mechanism, or their combination occur just for some cases with high shear forces.
- To investigate design resistance of cellular beam-columns, the design interaction resistances were computed from the three failure criteria, namely for flexural failure, Vierendeel mechanism, and web-post buckling. Cross-sectional properties at the opening centerline (2T section method) were conservatively used for computing the nominal flexure, shear and axial (for



the flexural buckling) strength. Vierendeel mechanism and web-post buckling criteria were modified to include effects of the flexural moment and the compressive axial load by using a quadratic interaction criterion.

- Generally, the design shear resistance based on criteria of the flexural behavior and Vierendeel mechanism conservatively agree well with the FE results. Differences of the critical design resistances from the FE resistances are in the range from -2.1% (conservative) to -36.0% for the flexural behavior, and from -32.0% to +3.6% (overestimated) for Vierendeel mechanism.
- Without consideration of the co-existing actions, the shear resistance of the web-post buckling based on SCI P355 tends to be overestimated, even by more than 50% in some cases. Based on an empirical study, the interaction criterion for the web-post buckling with high shear forces (ratio of shear force to shear strength of the web-post buckling higher than 0.5) was proposed. The proposed design resistances are better in line with the FE results for cases with web-post buckling failure. Differences of the critical design resistances from the FE results are in the range from -23.8% to +23.7%. The resistances tend to be overestimated for sections with low web slenderness ratio.

Note that using of the 2T section method provides a low value of the cross-section properties. Therefore, the interaction results are conservative under the flexural behavior. For future work the other methods such as Plain web section method, Surface weighting method, and Linear weighting method should be considered to investigate the design interaction resistances.

Author Contributions

P. Panedpojaman played a role in conceptualization, methodology, software, implementing the numerical model, interpreting the numerical results, validation, formal analysis, visualization, partially writing the manuscript, supervision, and project administration; W. Sae-Long played a role in methodology, software, interpreting the numerical results, validation, formal analysis, visualization, and partially writing the manuscript; R. Yapa played a role in software, interpreting the numerical results, and visualization; P. Chaiviriyawong played a role in revising the manuscript and investigation. The manuscript was written through the contribution of all authors. All authors discussed the results, reviewed, and approved the final version of the manuscript.

Acknowledgments

The authors sincerely thank Assoc. Prof. Dr. Seppo Karrila and the copy-editing service of the Research and Development Office, the Prince of Songkla University for their support and valuable comments.

Conflict of Interest

The authors declared no potential conflicts of interest concerning the research, authorship, and publication of this article.

Funding

The authors received no financial support for the research, authorship, and publication of this article.

Data Availability Statements

The datasets generated and/or analyzed during the current study are available from the corresponding author on reasonable request.

References


- [1] Nawar, M.T., Arafa, I.T., Elhosseiny, O., Numerical investigation on effective spans ranges of perforated steel beams, *Structures*, 25, 2020, 398-410.
- [2] Moghbeli, A., Sharifi, Y., New predictive equations for lateral-distortional buckling capacity assessment of cellular steel beams, *Structures*, 29, 2021, 911-923.
- [3] Lawson, R.M., Hicks, S.J., *Design of composite beams with large openings*, SCI P355, SCI Publication, Berkshire UK, 2011.
- [4] Khatri, A.P., Katikala, S.R., Kotapati, V.K., Effect of load height on elastic buckling behavior of I-shaped cellular beams, *Structures*, 33, 2021, 1923-1935.
- [5] Rodolpho, T.F., Rossi, A., Silva de Carvalho, A., Martins, C.H., Numerical analysis of the global stability of simply supported cellular steel columns under axial compression, *Thin-Walled Structures*, 192, 2023, 111143.
- [6] Sweedan, A.M.I., El-Sawy, K.M., Martini, M.I., Identification of the buckling capacity of axially loaded cellular columns, *Thin-Walled Structures*, 47(4), 2009, 442-454.
- [7] El-Sawy, K.M., Sweedan, A.M.I., Martini, M.I., Major-axis elastic buckling of axially loaded castellated steel columns, *Thin-Walled Structures*, 47(11), 2009, 1295-1304.
- [8] Yuan, W.-B., Kim, B., Li, L.-Y., Buckling of axially loaded castellated steel columns, *Journal of Constructional Steel Research*, 92, 2014, 40-45.
- [9] Gu, J.-Z., Cheng, S., Shear effect on buckling of cellular columns subjected to axially compressed load, *Thin-Walled Structures*, 98, 2016, 416-420.
- [10] Panedpojaman, P., Thepchatri, T., Limkatanyu, S., Elastic buckling of cellular columns under axial compression, *Thin-Walled Structures*, 145, 2019, 106434.
- [11] Sonck, D., Belis, J., Weak-axis flexural buckling of cellular and castellated columns, *Journal of Constructional Steel Research*, 124, 2016, 91-100.
- [12] CEN, EN 1993-1-1 Eurocode 3: *Design of Steel Structures - Part 1-1: General Rules and Rules for Buildings*, 2005.
- [13] ANSI/AISC 360-16, *Specification for structural steel buildings*, Chicago, Illinois: American Institute of Steel Construction, 2016.
- [14] Panedpojaman, P., Sae-Long, W., Thepchatri, T., Design of cellular beam-columns about the major axis, *Engineering Structures*, 236, 2021, 112060.
- [15] Belega, B., Manglekar H.C., Ray, T., Effects of axial-shear-flexure interaction in static and dynamic responses of steel beams, *Journal of Constructional Steel Research*, 131, 2017, 83-93.
- [16] Basler, K., Strength of plate girders under combined bending and shear, *Journal of the Structural Division*, 87(7), 1961, 181-197.
- [17] Bleich, F., *Buckling Strength of Metal Structures*, McGraw Hill, New York, USA, 1952.
- [18] Shahabian, F., Roberts, T.M., Behaviour of plate girders subjected to combined bending and shear loading, *Scientia Iranica*, 15(1), 2008, 16-20.
- [19] Silva de Carvalho, A., Rossi, A., Martins, C.H., Assessment of lateral-torsional buckling in steel I-beams with sinusoidal web openings, *Thin-Walled Structures*, 175, 2022, 109242.
- [20] Panedpojaman, P., Thepchatri, T., Limkatanyu, S., Novel simplified equations for Vierendeel design of beams with (elongated) circular openings, *Journal of Constructional Steel Research*, 112, 2015, 10-21.
- [21] Ward, J.K., *Design of composite and non-composite cellular beams*, SCI P100, SCI Publication, Berkshire UK, 1990.
- [22] Panedpojaman, P., Simplified equations for vierendeel design calculations of composite beams with web openings, *Steel and Composite Structures*, 27(4), 2018, 401-416.
- [23] Redwood, R.G., *Design of beams with web holes*, Canadian Steel Industries Construction Council, 1973.





- [24] Tsavdaridis, K.D., D'Mello, C., Web buckling study of the behaviour and strength of perforated steel beams with different novel web opening shapes, *Journal of Constructional Steel Research*, 67(10), 2011, 1605-1620.
- [25] ECSC, *Large web openings for service integration in composite floors*, Final Report for ECSC Research Contract 7210-PR-315, 2003.
- [26] Warren, J., *Ultimate load and deflection behaviour of cellular beams*, MSc Thesis, School of Civil Engineering, University of Natal, Durban, Republic of South Africa, 2001.
- [27] Erdal, F., Saka, M.P., Ultimate load carrying capacity of optimally designed steel cellular beams, *Journal of Constructional Steel Research*, 80, 2013, 355-368.
- [28] Neslušán, M., Jurkovic, M., Kalina, T. Pitonák, M., Zgútová, K., Monitoring of S235 steel over-stressing by the use of Barkhausen noise technique, *Engineering Failure Analysis*, 117, 2020, 104843.
- [29] Nseir, J., Lo, M., Sonck, D., Somja, H., Vassart, O., Boissonnade, N., Lateral torsional buckling of cellular beams, *Proceedings of the structural stability research council annual stability conference (SSRC2012)*, Grapevine, Texas, 2012.
- [30] Panedpojaman, P., Sae-Long, W., Chub-uppakarn, T., Cellular beam design for resistance to inelastic lateral-torsional buckling, *Thin-Walled Structures*, 99, 2016, 182-194.
- [31] Panedpojaman, P., Thepchatri, T., Limkatanyu, S., Novel design equations for shear strength of local web-post buckling in cellular beams, *Thin-Walled Structures*, 76, 2014, 92-104.

ORCID iD

Pattamad Panedpojaman  <https://orcid.org/0000-0002-7826-8547>

Worathep Sae-Long  <https://orcid.org/0000-0001-8149-4409>

Ruslan Yapa  <https://orcid.org/0009-0009-1153-2268>

Passagorn Chaiviriyawong  <https://orcid.org/0009-0007-3383-4254>



© 2024 Shahid Chamran University of Ahvaz, Ahvaz, Iran. This article is an open access article distributed under the terms and conditions of the Creative Commons Attribution-NonCommercial 4.0 International (CC BY-NC 4.0 license) (<http://creativecommons.org/licenses/by-nc/4.0/>).

How to cite this article: Panedpojaman P, Sae-Long W, Yapa R., Chaiviriyawong P. Design of Cellular Members under Axial-Shear-Flexure Interaction, *J. Appl. Comput. Mech.*, xx(x), 2024, 1-16. <https://doi.org/10.22055/jacm.2024.45237.4335>

Publisher's Note Shahid Chamran University of Ahvaz remains neutral with regard to jurisdictional claims in published maps and institutional affiliations.

